Search for Dark Matter Annihilations in the Sun with the 79-String IceCube Detector

M. G. Aartsen,[2] R. Abbasi,[27] Y. Abdou,[22] M. Ackermann,[41] J. Adams,[15] J. A. Aguilar,[21] M. Ahlers,[27] D. Altmann,[9] J. Auffenberg,[27] X. Bai,[31,*] M. Baker,[27] S. W. Barwick,[23] V. Baum,[28] R. Bay,[7] K. Beattie,[8] J. J. Beatty,[17,18] S. Bechet,[12] J. Becker Tjus,[10] K.-H. Becker,[40] M. Bell,[38] M. L. Benabderrahmane,[41] S. BenZvi,[27] J. Berdermann,[41] P. Berghaus,[41] D. Berley,[16] E. Bernardini,[41] A. Bernhard,[30] D. Bertrand,[12] D. Z. Besson,[25] D. Bindig,[40] M. Bissok,[1] E. Blaufuss,[16] J. Blumenthal,[1] D. J. Boersma,[39,1] S. Bohaichuk,[20] C. Bohm,[34] D. Bose,[13] S. Böser,[11] O. Botner,[39] L. Brayeur,[13] A. M. Brown,[15] R. Bruijn,[24] J. Brunner,[41] S. Buitink,[13] M. Carson,[22] J. Casey,[5] M. Casier,[13] D. Chirkin,[27] B. Christy,[16] K. Clark,[38] F. Clevermann,[19] S. Cohen,[24] D. F. Cowen,[38,37] A. H. Cruz Silva,[41] M. Danninger,[34] J. Daughhetee,[5] J. C. Davis,[17] C. De Clercq,[13] S. De Ridder,[22] P. Desiati,[27] G. de Vries-Uiterweerd,[22] M. de With,[9] T. DeYoung,[38] J. C. Díaz-Vélez,[27] J. Dreyer,[10] M. Dunkman,[38] R. Eagan,[38] B. Eberhardt,[28] J. Eisch,[27] R. W. Ellsworth,[16] O. Engdegård,[39] S. Euler,[1] P. A. Evenson,[31] O. Fadiran,[27] A. R. Fazely,[6] A. Fedynitch,[10] J. Feintzeig,[27] T. Feusels,[22] K. Filimonov,[7] C. Finley,[34] T. Fischer-Wasels,[40] S. Flis,[34] A. Franckowiak,[11] R. Franke,[41] K. Frantzen,[19] T. Fuchs,[19] T. K. Gaisser,[31] J. Gallagher,[26] L. Gerhardt,[8,7] L. Gladstone,[27] T. Glüsenkamp,[41] A. Goldschmidt,[8] G. Golup,[13] J. A. Goodman,[16] D. Góra,[41] D. Grant,[20] A. Groß,[30] M. Gurtner,[40] C. Ha,[8,7] A. Haj Ismail,[22] A. Hallgren,[39] F. Halzen,[27] K. Hanson,[12] D. Heereman,[12] P. Heimann,[1] D. Heinen,[1] K. Helbing,[40] R. Hellauer,[16] S. Hickford,[15] G. C. Hill,[2] K. D. Hoffman,[16] R. Hoffmann,[40] A. Homeier,[11] K. Hoshina,[27] W. Huelsnitz,[16,†] P. O. Hulth,[34] K. Hultqvist,[34] S. Hussain,[31] A. Ishihara,[14] E. Jacobi,[41] J. Jacobsen,[27] G. S. Japaridze,[4] K. Jero,[27] O. Jlelati,[22] B. Kaminsky,[41] A. Kappes,[9] T. Karg,[41] A. Karle,[27] J. L. Kelley,[27] J. Kiryluk,[35] F. Kislat,[41] J. Kläs,[40] S. R. Klein,[8,7] J.-H. Köhne,[19] G. Kohnen,[29] H. Kolanoski,[9] L. Köpke,[28] C. Kopper,[27] S. Kopper,[40] D. J. Koskinen,[38] M. Kowalski,[11] M. Krasberg,[27] G. Kroll,[28] J. Kunnen,[13] N. Kurahashi,[27] T. Kuwabara,[31] M. Labare,[13] H. Landsman,[27] M. J. Larson,[36] M. Lesiak-Bzdak,[35] J. Leute,[30] J. Lünemann,[28] J. Madsen,[33] R. Maruyama,[27] K. Mase,[14] H. S. Matis,[8] F. McNally,[27] K. Meagher,[16] M. Merck,[27] P. Mészáros,[37,38] T. Meures,[12] S. Miarecki,[8,7] E. Middell,[41] N. Milke,[19] J. Miller,[13] L. Mohrmann,[41] T. Montaruli,[21,‡] R. Morse,[27] R. Nahnhauer,[41] U. Naumann,[40] H. Niederhausen,[35] S. C. Nowicki,[20] D. R. Nygren,[8] A. Obertacke,[40] S. Odrowski,[30] A. Olivas,[16] M. Olivo,[10] A. O'Murchadha,[12] L. Paul,[1] J. A. Pepper,[36] C. Pérez de los Heros,[39] C. Pfendner,[17] D. Pieloth,[19] N. Pirk,[41] J. Posselt,[40] P. B. Price,[7] G. T. Przybylski,[8] L. Rädel,[1] K. Rawlins,[3] P. Redl,[16] E. Resconi,[30] W. Rhode,[19] M. Ribordy,[24] M. Richman,[16] B. Riedel,[27] J. P. Rodrigues,[27] C. Rott,[17] T. Ruhe,[19] B. Ruzybayev,[31] D. Ryckbosch,[22] S. M. Saba,[10] T. Salameh,[38] H.-G. Sander,[28] M. Santander,[27] S. Sarkar,[32] K. Schatto,[28] M. Scheel,[1] F. Scheriau,[19] T. Schmidt,[16] M. Schmitz,[19] S. Schoenen,[1] S. Schöneberg,[10] L. Schönherr,[1] A. Schönwald,[41] A. Schukraft,[1] L. Schulte,[11] O. Schulz,[30] D. Seckel,[31] S. H. Seo,[34] Y. Sestayo,[30] S. Seunarine,[33] C. Sheremata,[20] M. W. E. Smith,[38] M. Soiron,[1] D. Soldin,[40] G. M. Spiczak,[33] C. Spiering,[41] M. Stamatikos,[17,§] T. Stanev,[31] A. Stasik,[11] T. Stezelberger,[8] R. G. Stokstad,[8] A. Stößl,[41] E. A. Strahler,[13] R. Ström,[39] G. W. Sullivan,[16] H. Taavola,[39] I. Taboada,[5] A. Tamburro,[31] S. Ter-Antonyan,[6] S. Tilav,[31] P. A. Toale,[36] S. Toscano,[27] M. Usner,[11] D. van der Drift,[8,7] N. van Eijndhoven,[13] A. Van Overloop,[22] J. van Santen,[27] M. Vehring,[1] M. Voge,[11] M. Vraeghe,[22] C. Walck,[34] T. Waldenmaier,[9] M. Wallraff,[1] R. Wasserman,[38] Ch. Weaver,[27] M. Wellons,[27] C. Wendt,[27] S. Westerhoff,[27] N. Whitehorn,[27] K. Wiebe,[28] C. H. Wiebusch,[1] D. R. Williams,[36] H. Wissing,[16] M. Wolf,[34] T. R. Wood,[20] K. Woschnagg,[7] C. Xu,[31] D. L. Xu,[36] X. W. Xu,[6] J. P. Yanez,[41] G. Yodh,[23] S. Yoshida,[14] P. Zarzhitsky,[36] J. Ziemann,[19] S. Zierke,[1] A. Zilles,[1] and M. Zoll[34]

(IceCube Collaboration)

[1]*III. Physikalisches Institut, RWTH Aachen University, D-52056 Aachen, Germany*
[2]*School of Chemistry and Physics, University of Adelaide, Adelaide, South Australia 5005, Australia*
[3]*Department of Physics and Astronomy, University of Alaska Anchorage, 3211 Providence Drive, Anchorage, Alaska 99508, USA*
[4]*CTSPS, Clark-Atlanta University, Atlanta, Georgia 30314, USA*
[5]*School of Physics and Center for Relativistic Astrophysics, Georgia Institute of Technology, Atlanta, Georgia 30332, USA*
[6]*Department of Physics, Southern University, Baton Rouge, Louisiana 70813, USA*
[7]*Department of Physics, University of California, Berkeley, California 94720, USA*
[8]*Lawrence Berkeley National Laboratory, Berkeley, California 94720, USA*
[9]*Institut für Physik, Humboldt-Universität zu Berlin, D-12489 Berlin, Germany*
[10]*Fakultät für Physik und Astronomie, Ruhr-Universität Bochum, D-44780 Bochum, Germany*
[11]*Physikalisches Institut, Universität Bonn, Nussallee 12, D-53115 Bonn, Germany*
[12]*Université Libre de Bruxelles, Science Faculty CP230, B-1050 Brussels, Belgium*

[13]Vrije Universiteit Brussel, Dienst ELEM, B-1050 Brussels, Belgium
[14]Department of Physics, Chiba University, Chiba 263-8522, Japan
[15]Department of Physics and Astronomy, University of Canterbury, Private Bag 4800, Christchurch, New Zealand
[16]Department of Physics, University of Maryland, College Park, Maryland 20742, USA
[17]Department of Physics and Center for Cosmology and Astro-Particle Physics, Ohio State University, Columbus, Ohio 43210, USA
[18]Department of Astronomy, Ohio State University, Columbus, Ohio 43210, USA
[19]Department of Physics, TU Dortmund University, D-44221 Dortmund, Germany
[20]Department of Physics, University of Alberta, Edmonton, Alberta T6G 2G7, Canada
[21]Département de physique nucléaire et corpusculaire, Université de Genève, CH-1211 Genève, Switzerland
[22]Department of Physics and Astronomy, University of Gent, B-9000 Gent, Belgium
[23]Department of Physics and Astronomy, University of California, Irvine, California 92697, USA
[24]Laboratory for High Energy Physics, École Polytechnique Fédérale, CH-1015 Lausanne, Switzerland
[25]Department of Physics and Astronomy, University of Kansas, Lawrence, Kansas 66045, USA
[26]Department of Astronomy, University of Wisconsin, Madison, Wisconsin 53706, USA
[27]Department of Physics and Wisconsin IceCube Particle Astrophysics Center, University of Wisconsin, Madison, Wisconsin 53706, USA
[28]Institute of Physics, University of Mainz, Staudinger Weg 7, D-55099 Mainz, Germany
[29]Université de Mons, 7000 Mons, Belgium
[30]Technical University of Munich, D-85748 Garching, Germany
[31]Bartol Research Institute and Department of Physics and Astronomy, University of Delaware, Newark, Delaware 19716, USA
[32]Department of Physics, University of Oxford, 1 Keble Road, Oxford OX1 3NP, United Kingdom
[33]Department of Physics, University of Wisconsin, River Falls, Wisconsin 54022, USA
[34]Oskar Klein Centre and Department of Physics, Stockholm University, SE-10691 Stockholm, Sweden
[35]Department of Physics and Astronomy, Stony Brook University, Stony Brook, New York 11794-3800, USA
[36]Department of Physics and Astronomy, University of Alabama, Tuscaloosa, Alabama 35487, USA
[37]Department of Astronomy and Astrophysics, Pennsylvania State University, University Park, Pennsylvania 16802, USA
[38]Department of Physics, Pennsylvania State University, University Park, Pennsylvania 16802, USA
[39]Department of Physics and Astronomy, Uppsala University, Box 516, S-75120 Uppsala, Sweden
[40]Department of Physics, University of Wuppertal, D-42119 Wuppertal, Germany
[41]DESY, D-15735 Zeuthen, Germany

(Received 17 December 2012; revised manuscript received 20 February 2013; published 28 March 2013)

We have performed a search for muon neutrinos from dark matter annihilation in the center of the Sun with the 79-string configuration of the IceCube neutrino telescope. For the first time, the DeepCore subarray is included in the analysis, lowering the energy threshold and extending the search to the austral summer. The 317 days of data collected between June 2010 and May 2011 are consistent with the expected background from atmospheric muons and neutrinos. Upper limits are set on the dark matter annihilation rate, with conversions to limits on spin-dependent and spin-independent scattering cross sections of weakly interacting massive particles (WIMPs) on protons, for WIMP masses in the range 20–5000 GeV$/c^2$. These are the most stringent spin-dependent WIMP-proton cross section limits to date above 35 GeV$/c^2$ for most WIMP models.

DOI: 10.1103/PhysRevLett.110.131302 PACS numbers: 95.35.+d, 14.80.Nb, 14.80.Rt, 96.50.S−

While the presence of dark matter (DM) in the Universe has been inferred through its gravitational interactions, its nature remains a mystery. One of the most promising and experimentally accessible candidates for DM is the so-called weakly interacting massive particle (WIMP) [1], predicted in extensions of the standard model (SM) of particle physics. DM may be captured in large celestial bodies like the Sun [2] where self-annihilation to SM particles can result in a flux of high-energy neutrinos. These neutrinos can be searched for as a pointlike source by IceCube [3,4]. These indirect searches for DM are sensitive to the WIMP-proton scattering cross section, which initiates the capture process in the Sun. They complement direct DM searches on Earth as they scale with the averaged DM density along the solar circle and are more sensitive to low WIMP velocities [5]. Indirect searches depend only weakly on the underlying WIMP velocity distribution [6], and we have chosen parameters to be conservative in our analysis.

In this work, we present new IceCube limits on dark matter captured by the Sun, with data taken in the 79-string configuration of the detector. This analysis incorporates two significant additions compared to previous work. First, we extend the search to the austral summer when the Sun is above the horizon. This doubles the live time of the analysis but imposes new challenges to reduce the down-going atmospheric muon background. Second, we search for neutrinos from WIMPs with masses (m_χ) as low as 20 GeV$/c^2$, whereas past IceCube searches have only been sensitive above 50 GeV$/c^2$.

The IceCube detector [7] is situated at the South Pole. Digital optical modules (DOMs) arranged on vertical strings deep in the ice sheet record the Cherenkov light emitted by relativistic charged particles, including those created in neutrino interactions in the ice. The detection of photon yields and arrival times in DOMs allows the reconstruction of direction and energy of the secondaries. This analysis used 317 live days of data taken between June 2010 and May 2011. During this period, the detector was operating in its 79-string configuration, which includes six more densely instrumented strings in the center of the array, optimized for low energies. These strings feature reduced vertical spacing between DOMs and higher quantum efficiency photomultiplier tubes. Along with the seven surrounding regular strings, they form the DeepCore subarray [8]. Both the improvement in live time and in energy threshold, which this analysis has achieved over previous IceCube analyses, can be attributed to the use of the DeepCore array.

All signal simulations are made with DarkSUSY [9] and WimpSim [10], which describe the capture and annihilation of WIMPs inside the Sun and the consequent production, interaction, and propagation of neutrinos from the core of the Sun to the detector, including three-flavor oscillations and matter effects. The primary WIMP annihilation spectrum is very model dependent, owing to different branching ratios into SM particles. We approximately bracket the range of possible models by assuming 100% branching into two channels with very different characteristics: the "hard" channel $\chi\chi \rightarrow W^+W^-$ ($\tau^+\tau^-$ below $m_\chi = 80.4$ GeV$/c^2$) and the "soft" channel $\chi\chi \rightarrow b\bar{b}$. For this work, WIMP masses ranging from 20 GeV$/c^2$ to 5 TeV$/c^2$ are simulated.

The background in this search consists of muons and neutrinos created in cosmic ray interactions in Earth's atmosphere. The dominant down-going muon component is simulated with CORSIKA [11], including simulations of single and coincident air showers. The ν_μ and ν_e components of the atmospheric spectrum are generated following the Honda flux model [12]. For verification and cross-checks, a dedicated simulation of atmospheric ν's below 200 GeV$/c^2$ is performed with GENIE [13]. The background at the final analysis level from solar atmospheric neutrinos, originating from cosmic ray interactions in the Sun's atmosphere, has been calculated to be of an order 1 event, independent of the flux model [14–16]. To reduce the dependence on simulation and associated systematic errors, we use off-source data to estimate the background at all analysis levels. Background simulation is merely used to verify accurate understanding of the detector. Off-source data consist of data recorded when the Sun was outside the respective analysis region.

Propagation of muons through the ice is simulated [17], and transport of light from these particles to the DOMs is performed using direct photon tracking [18], taking into account measured ice properties [19]. Particle and photon propagation simulations at the lowest targeted energies below 50 GeV$/c^2$ have been independently verified using GEANT4 [20].

In this work, the full data set is split into three independent nonoverlapping event selections, first into "summer" and "winter" seasons, when the Sun is above and below the horizon, respectively. The winter data set is further split into a low energy sample (WL), with focus on neutrino-induced muon tracks starting within DeepCore, and a higher energy sample (WH), aiming to select tracklike events with no particular containment requirement. The summer selection is a dedicated low energy event sample (SL) for which the surrounding IceCube strings are used as an active muon veto in order to select neutrino-induced events, starting within DeepCore. Separation into these samples is necessary, owing to the different characteristics of the overwhelming down-going muon background within each data set. The event selection is carried out separately for each independent sample, and the final search is conducted using a combined likelihood function. In order to avoid potential bias, a strict blindness criterion is imposed by scrambling the azimuthal position of the Sun in data.

In IceCube, filters preselect data to enhance the content of signal-like muon events above the dominant atmospheric muon background. To increase the signal-to-background ratio, we only select events that pass any of three filters: the dedicated DeepCore low energy filter [8] and two filters selecting muonlike events with an upward pointing track reconstruction. At this point, the data set is split into the two seasonal streams, where September 22nd, 2010, and March 22nd, 2011, mark the beginning and ending dates of the SL selection. We first discuss the additional winter cut selections: Cuts are applied on the zenith angle and quality of the likelihood-based track reconstruction, on hit and string multiplicity, and on timing and topological variables. For DeepCore contained events, the zenith acceptance region is extended to reflect the broadened signal point spread function at low energies.

The first data reduction is followed by additional processing, including an estimate of the angular uncertainty of the muon track fit. Some signal neutrinos will arrive in coincidence with atmospheric backgrounds (10%). In order to retain these signal events, a set of topological criteria is applied to "split" these combined hit patterns into distinct subevents. These subevents are then processed as above and undergo all subsequent event selection in their own right. Following the addition of events from splitting, the data set is divided into independent low and high energy event samples. For events to be included in the WL sample, we demand that the number of hit DOMs within DeepCore must be larger than outside. Additionally, the number of outside hits must be less than seven. This ensures that events with a long lever arm and therefore good angular resolution are assigned to the complement

sample. Events that fail the WL criteria are classified as WH events and undergo a series of additional, stricter cuts on the same variables as in the initial event selection. WL events, conversely, undergo a veto cut, removing events with hits in the ten uppermost layers of DOMs on the regular (non-DeepCore) strings. The final background reduction utilizes one boosted decision tree (BDT) [21] for each data set to discriminate true up-going muonlike events from misreconstructed atmospheric muons. For training and testing, an independent high statistics set of signal simulations is used and discarded afterward. For background training, this multivariate analysis uses one month of off-source data. Through an iterative process, individual variables were removed and added and the performance of the BDT evaluated, until we arrived at a final set of 14 variables in the WH stream and 10 in the WL stream. All input distributions for simulated backgrounds and data are in good agreement. The selected variables describe both the quality of the track reconstruction and the time evolution of the pattern of hit DOMs and spatial positions within the detector.

The SL event sample uses a different set of cuts because the dominant background is comprised of well-reconstructed down-going muons penetrating the detector. To reduce these backgrounds, we focus on low m_χ signals with a reconstructed neutrino interaction vertex inside the DeepCore fiducial volume. Selecting only these events, cuts are placed on the zenith angle of the track reconstruction, hit multiplicity, and vertical extension of the event. A 14 DOM layer top veto is imposed to reject down-going events. Additionally, events are required to be DeepCore dominated (defined in the same way as for the winter analysis) and fulfill a tight hit-time containment criterion. The final step in background rejection again consists of one BDT with ten input variables. These are selected using the same iterative selection process. Track quality parameters yield less separation power within this down-going sample. As a result, the final BDT input observables mainly describe the degree of containment and the vertical and lateral extension of the event within the detector.

The cut on the BDT score is optimized for each event selection to minimize the model rejection factor [22] in the full likelihood analysis. Total signal cut efficiencies range between 1% and 5% for low m_χ signals and up to 30%–40% for high m_χ. The final step of the analysis is a likelihood ratio hypothesis test based on the values of the reconstructed angle to the Sun Ψ, using the Feldman-Cousins unified approach [23]. This results in confidence intervals for the mean number of signal events μ_s. The required probability densities for signal are computed from simulations, while for background they are based on real data events at the final selection level, with a scrambled azimuth direction. A single result is calculated from all three data samples with a combined likelihood, constructed from the set of three independent probability distributions of signal and background, weighting each by the respective live time and effective volume (see Ref. [4] for details).

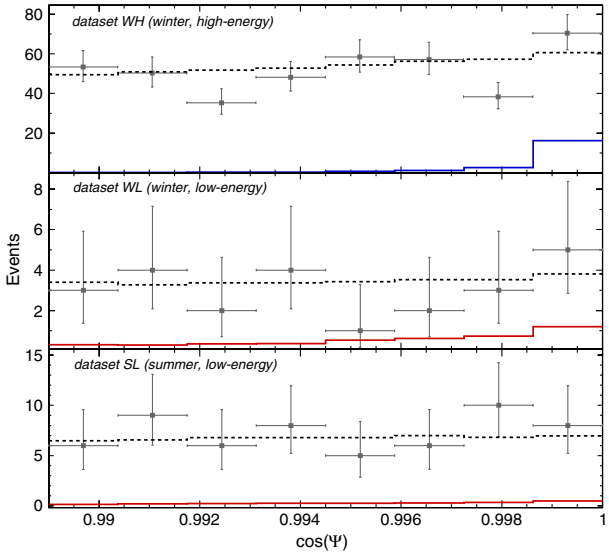

FIG. 1 (color online). Cosine of the angle between the reconstructed track and the direction of the Sun Ψ for observed events (squares), with 1 standard deviation error bars and the atmospheric background expectation from atmospheric muons and neutrinos (dashed line). Also shown is a simulated signal (1 TeV/c^2 hard for data set WH, 50 GeV/c^2 hard for data sets WL and SL) scaled to μ_s^{90} (details are given in Table I).

After unblinding the direction of the events in the final data samples, the observed distributions are compared to the expected background distributions from atmospheric muons and neutrinos, shown in Fig. 1. The observed number of events from the direction of the Sun is consistent with the background-only hypothesis. The upper 90% C.L. limits on μ_s are calculated and listed for each signal hypothesis in Table I.

The upper limit on μ_s can be translated into a limit on the signal flux and annihilation rate in the Sun. The effect of different sources of systematic uncertainties on signal flux expectations is calculated for three signal energy regions, defined in Table II by corresponding benchmark WIMP masses. Sources of uncertainties are divided into two classes, measurement and parametrization errors on cross sections and neutrino properties on the one hand and limitations in the detector simulation and uncertainties in detector calibrations on the other hand. The first class, class I, affects signal normalizations only, whereas the latter (class II) alters signal acceptance and introduces changes in the point spread function that is the basis for the likelihood analysis. Class-II uncertainties are evaluated using alternative signal simulations with varied calibration parameters, processed through the same analysis chain and evaluated with the full multi-data-set combined likelihood. This procedure explicitly determines the systematic effect on μ_s.

TABLE I. Results from the combination of the three independent data sets. The upper 90% limits on the number of signal events μ_s^{90}, the WIMP annihilation rate in the Sun Γ_A, the muon flux Φ_μ and neutrino flux Φ_ν, and the WIMP-proton scattering cross sections (spin independent, $\sigma_{\mathrm{SI},p}$; spin dependent, $\sigma_{\mathrm{SD},p}$) at the 90% confidence level, including systematic errors. The sensitivity $\bar{\Phi}_\mu$ (see the text) is shown for comparison.

m_χ (GeV/c^2)	Channel	μ_s^{90}	Γ_A (s^{-1})	$\bar{\Phi}_\mu$ (km$^{-2}y^{-1}$)	Φ_μ (km$^{-2}y^{-1}$)	Φ_ν (km$^{-2}y^{-1}$)	$\sigma_{\mathrm{SI},p}$ (cm^2)	$\sigma_{\mathrm{SD},p}$ (cm^2)
20	$\tau^+\tau^-$	162	2.46×10^{25}	5.26×10^{4}	9.27×10^{4}	2.35×10^{15}	1.08×10^{-40}	1.29×10^{-38}
35	$\tau^+\tau^-$	70.2	1.03×10^{24}	1.03×10^{4}	1.21×10^{4}	1.02×10^{14}	6.59×10^{-42}	1.28×10^{-39}
35	$b\bar{b}$	128	1.99×10^{26}	5.63×10^{4}	1.04×10^{5}	6.29×10^{15}	1.28×10^{-39}	2.49×10^{-37}
50	$\tau^+\tau^-$	19.6	1.20×10^{23}	4.82×10^{3}	2.84×10^{3}	1.17×10^{13}	1.03×10^{-42}	2.70×10^{-40}
50	$b\bar{b}$	55.2	1.75×10^{25}	2.06×10^{4}	1.80×10^{4}	5.64×10^{14}	1.51×10^{-40}	3.96×10^{-38}
100	W^+W^-	16.8	3.35×10^{22}	1.49×10^{3}	1.19×10^{3}	1.23×10^{12}	6.01×10^{-43}	2.68×10^{-40}
100	$b\bar{b}$	28.9	1.82×10^{24}	7.57×10^{3}	5.91×10^{3}	6.34×10^{13}	3.30×10^{-41}	1.47×10^{-38}
250	W^+W^-	29.9	2.85×10^{21}	3.04×10^{2}	4.15×10^{2}	9.72×10^{10}	1.67×10^{-43}	1.34×10^{-40}
250	$b\bar{b}$	19.8	1.27×10^{23}	1.85×10^{3}	1.45×10^{3}	4.59×10^{12}	7.37×10^{-42}	5.90×10^{-39}
500	W^+W^-	25.2	8.57×10^{20}	1.46×10^{2}	2.23×10^{2}	2.61×10^{10}	1.45×10^{-43}	1.57×10^{-40}
500	$b\bar{b}$	30.6	4.12×10^{22}	8.53×10^{2}	1.02×10^{3}	1.52×10^{12}	6.98×10^{-42}	7.56×10^{-39}
1000	W^+W^-	23.4	6.13×10^{20}	1.19×10^{2}	1.85×10^{2}	1.62×10^{10}	3.46×10^{-43}	4.48×10^{-40}
1000	$b\bar{b}$	30.4	1.39×10^{22}	4.33×10^{2}	5.99×10^{2}	5.23×10^{11}	7.75×10^{-42}	1.00×10^{-38}
3000	W^+W^-	22.2	7.79×10^{20}	1.09×10^{2}	1.66×10^{2}	1.65×10^{10}	3.44×10^{-42}	5.02×10^{-39}
3000	$b\bar{b}$	26.1	4.88×10^{21}	2.52×10^{2}	3.47×10^{2}	1.89×10^{11}	2.17×10^{-41}	3.16×10^{-38}
5000	W^+W^-	22.8	8.79×10^{20}	1.01×10^{2}	1.58×10^{2}	1.77×10^{10}	1.06×10^{-41}	1.59×10^{-38}
5000	$b\bar{b}$	26.4	6.50×10^{20}	2.21×10^{2}	3.26×10^{2}	1.63×10^{11}	4.89×10^{-41}	7.29×10^{-38}

Uncertainties in neutrino-nucleon cross sections for signal simulations arise in the parametrization of the CTEQ6-DIS parton distribution functions as used in NUSIGMA [24]. In addition to this theoretical uncertainty on σ_ν, the energy-dependent error on the experimental σ_ν measurement [25] is included. The uncertainty in neutrino oscillation parameters used in signal flux calculations is investigated through variations of mixing parameters within the quoted 1σ regions [25]. Here, the dominant effect results from the least constrained mixing angle θ_{23}, maximizing tau (dis)appearance within the expected flux expectation.

The second class of uncertainties includes absolute calibration and DOM to DOM variation of sensitivity, optical properties of the glacial ice, and photon propagation to the detector. The systematic uncertainties on absolute DOM sensitivity are evaluated with sets of signal simulations with an overall shift of 10% in DOM efficiency. As baseline simulations do not account for varying relative DOM efficiency, dedicated signal simulations are performed with individual DOM efficiencies from a Gaussian fitted to the *in situ* measured spread ($\sigma = 0.087$) and centered around the nominal value. Optical properties of the glacial ice are measured [19] and characterized in models that are parametrizations of the absorption and scattering coefficients as a function of depth and position in the detector. Two such models [19,26], differing in parametrization techniques, are considered to bracket the uncertainty in light yield resulting from the ice description. Individual uncertainties, listed in Table II, are added in quadrature to obtain the total systematic uncertainty for each benchmark mass region.

The upper limits on μ_s for each signal hypothesis are then converted to limits on the neutrino to muon conversion rate and, through DarkSUSY [9], to limits on the WIMP annihilation rate in the Sun Γ_A. For better comparison to other experiment limits, the neutrino flux (Φ_ν) from the Sun and the corresponding induced muon flux in the ice (Φ_μ), both integrated above 1 GeV, are computed at the 90% confidence level. These limits are listed in Table I. Also specified is the median sensitivity $\bar{\Phi}_\mu$ derived from simulations without signal. Under the assumption of equilibrium between WIMP capture and annihilation in the Sun, limits on Γ_A are converted into limits on the spin-dependent $\sigma_{\mathrm{SD},p}$ and spin-independent $\sigma_{\mathrm{SI},p}$ WIMP-proton scattering cross sections, using the method from Ref. [27]. The results are listed in Table I and shown in Fig. 2 together

TABLE II. Systematic errors on signal flux expectations in %. The class-II uncertainties are marked with *'s

Source	Mass ranges (GeV/c^2) <35	35–100	>100
ν oscillations	6	6	6
ν-nucleon cross section	7	5.5	3.5
μ propagation in ice	<1	<1	<1
Time, position calibration	5	5	5
DOM sensitivity spread*	6	3	10
Photon propagation in ice*	15	10	5
Absolute DOM efficiency*	50	20	15
Total uncertainty	54	25	21

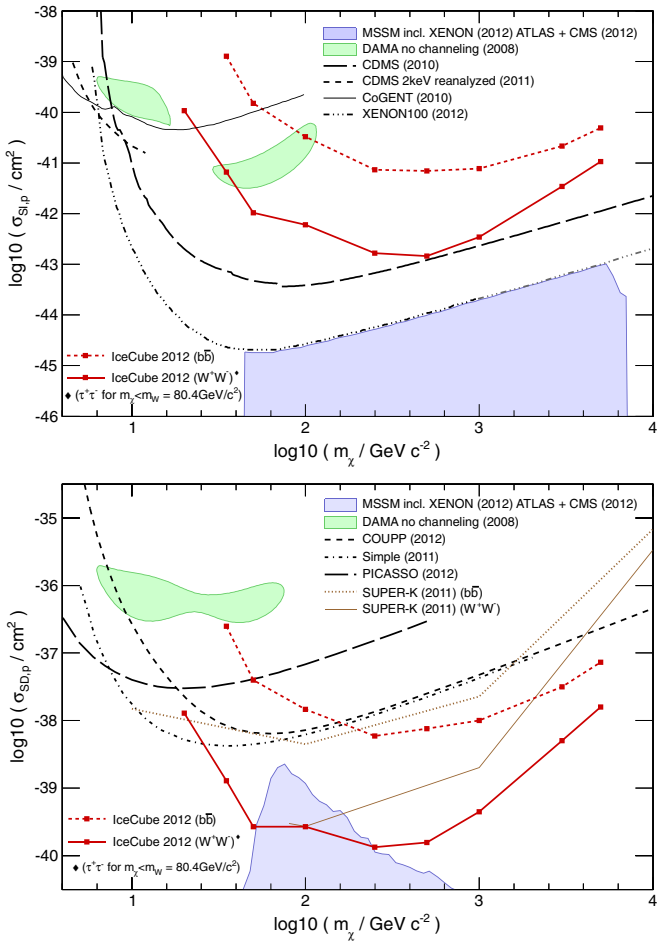

FIG. 2 (color online). 90% C.L. upper limits on $\sigma_{\mathrm{SI},p}$ (top figure) and $\sigma_{\mathrm{SD},p}$ (bottom figure) for hard and soft annihilation channels over a range of WIMP masses. Systematic uncertainties are included. The shaded region represents an allowed minimal supersymmetric standard model parameter space (MSSM-25 [42]) taking into account recent accelerator [43], cosmological, and direct DM search constraints. The results from Super-K [28], COUPP (exponential model) [29], PICASSO [30], CDMS [31,32], XENON100 (limits above 1 TeV/c^2 from the XENON100 Collaboration) [36], CoGeNT [35], Simple [37], and DAMA [33,34] are shown for comparison.

with other experimental limits [28–37]. We assume a standard DM halo with a local density of 0.3 GeV/cm3 [25] and a Maxwellian WIMP velocity distribution with an rms velocity of 270 km/s. We do not include the detailed effects of diffusion and planets upon the capture rate, as the simple free-space approximation [2] included in DarkSUSY is found to be accurate [38]. Limits on the WIMP-nucleon scattering cross section can also be deduced from limits on monojet and monophoton signals at hadron colliders, but these depend strongly on the choice of the underlying effective theory and mediator masses [39–41] and are consequently not included in Fig. 2.

In conclusion, we have presented the most stringent limits to date on the spin-dependent WIMP-proton cross section for WIMPs annihilating into W^+W^- or $\tau^+\tau^-$ with masses above 35 GeV/c^2. With this data set, we have demonstrated for the first time the ability of IceCube to probe WIMP masses below 50 GeV/c^2. This has been accomplished through effective use of the DeepCore subarray. Furthermore, we have accessed the southern sky for the first time by incorporating strong vetoes against the large atmospheric muon backgrounds. The added live time has been shown to improve the presented limits. IceCube has now achieved limits that strongly constrain dark matter models and that will impact global fits of the allowed dark matter parameter space. This impact will only increase in the future, as analysis techniques improve and detector live time increases.

We thank H. Silverwood for his support on SUSY model scans. We acknowledge the support from the following agencies: U.S. National Science Foundation-Office of Polar Programs, U.S. National Science Foundation-Physics Division, University of Wisconsin Alumni Research Foundation, the Grid Laboratory Of Wisconsin (GLOW) grid infrastructure at the University of Wisconsin-Madison, the Open Science Grid (OSG) grid infrastructure, U.S. Department of Energy, National Energy Research Scientific Computing Center, and the Louisiana Optical Network Initiative (LONI) grid computing resources; National Science and Engineering Research Council of Canada; Swedish Research Council, Swedish Polar Research Secretariat, Swedish National Infrastructure for Computing (SNIC), and Knut and Alice Wallenberg Foundation, Sweden; German Ministry for Education and Research (BMBF), Deutsche Forschungsgemeinschaft (DFG), Helmholtz Alliance for Astroparticle Physics (HAP), and Research Department of Plasmas with Complex Interactions (Bochum), Germany; Fund for Scientific Research (FNRS-FWO), FWO Odysseus programme, Flanders Institute to encourage scientific and technological research in industry (IWT), and Belgian Federal Science Policy Office (Belspo); University of Oxford, United Kingdom; Marsden Fund, New Zealand; Australian Research Council; Japan Society for Promotion of Science (JSPS); and the Swiss National Science Foundation (SNSF), Switzerland.

*Present address: Physics Department, South Dakota School of Mines and Technology, Rapid City, SD 57701, USA.
†Present address: Los Alamos National Laboratory, Los Alamos, NM 87545, USA.
‡Also at Sezione INFN, Dipartimento di Fisica, I-70126, Bari, Italy.
§Present address: NASA Goddard Space Flight Center, Greenbelt, MD 20771, USA.

[1] G. Bertone, D. Hooper, and J. Silk, Phys. Rep. **405**, 279 (2005).

[2] A. Gould, Astrophys. J. **328**, 919 (1988); J. Silk, K. Olive, and M. Srednicki, Phys. Rev. Lett. **55**, 257 (1985); T. K. Gaisser, G. Steigman, and S. Tilav, Phys. Rev. D **34**, 2206 (1986); W. H. Press and D. N. Spergel, Astrophys. J. **296**, 679 (1985).

[3] R. Abbasi *et al.*, Phys. Rev. Lett. **102**, 201302 (2009).

[4] R. Abbasi *et al.*, Phys. Rev. D **85**, 042002 (2012).

[5] T. Bruch, A. H. G. Peter, J. Read, L. Baudis, and G. Lake, Phys. Lett. B **674**, 250 (2009).

[6] C. Rott, T. Tanaka, and Y. Itow, J. Cosmol. Astropart. Phys. 09 (2011) 029.

[7] R. Abbasi *et al.*, Nucl. Instrum. Methods Phys. Res., Sect. A **618**, 139 (2010); R. Abbasi *et al.*, Nucl. Instrum. Methods Phys. Res., Sect. A **601**, 294 (2009).

[8] R. Abbasi *et al.*, Astropart. Phys. **35**, 615 (2012).

[9] P. Gondolo, J. Edsjö, P. Ullio, L. Bergström, M. Schelke, and E. A. Baltz, J. Cosmol. Astropart. Phys. 07 (2004) 008.

[10] M. Blennow, J. Edsjö, and T. Ohlsson, J. Cosmol. Astropart. Phys. 01 (2008) 021.

[11] D. Heck *et al.*, FZKA Report No. 6019, 1998.

[12] T. K. Gaisser and M. Honda, Annu. Rev. Nucl. Part. Sci. **52**, 153 (2002); M. Honda, T. Kajita, K. Kasahara, S. Midorikawa, and T. Sanuki, Phys. Rev. D **75**, 043006 (2007).

[13] C. Andreopoulos *et al.*, Nucl. Instrum. Methods Phys. Res., Sect. A **614**, 87 (2010).

[14] G. Ingelman and M. Thunman, Phys. Rev. D **54**, 4385 (1996).

[15] G. L. Fogli, E. Lisi, A. Mirizzi, D. Montanino, and P. Serpico, Phys. Rev. D **74**, 3004 (2006).

[16] C. Hettlage, K. Mannheim, and J. G. Learned, Astropart. Phys. **13**, 45 (2000).

[17] D. Chirkin and W. Rhode, arXiv:hep-ph/0407075v2.

[18] D. Chirkin, Nucl. Instrum. Methods Phys. Res., Sect. A, doi: 10.1016/j.nima.2012.11.170 (2012).

[19] M. Ackermann *et al.*, J. Geophys. Res. **111**, D13203 (2006).

[20] S. Agostinelli *et al.*, Nucl. Instrum. Methods Phys. Res., Sect. A **506**, 250 (2003).

[21] H. Voss *et al.*, Proc. Sci., ACAT (2007) 040; arXiv: physics/0703039v5.

[22] G. Hill and K. Rawlins, Astropart. Phys. **19**, 393 (2003).

[23] G. J. Feldman and R. D. Cousins, Phys. Rev. D **57**, 3873 (1998).

[24] J. Edsjö, The NUSIGMA Neutrino-Nucleon Scattering Monte Carlo, http://www.physto.se/edsjo.

[25] J. Beringer *et al.* (Particle Data Group), Phys. Rev. D **86**, 010001 (2012).

[26] M. G. Aartsen *et al.*, Nucl. Instrum. Methods Phys. Res., Sect. A **711**, 73 (2013).

[27] G. Wikström and J. Edsjö, J. Cosmol. Astropart. Phys. 04 (2009) 009.

[28] T. Tanaka *et al.*, Astrophys. J. **742**, 78 (2011).

[29] E. Behnke *et al.*, Phys. Rev. D **86**, 052001 (2012).

[30] S. Archambault *et al.*, Phys. Lett. B **711**, 153 (2012).

[31] Z. Ahmed *et al.* (The CDMS II Collaboration), Science **327**, 1619 (2010).

[32] Z. Ahmed *et al.*, Phys. Rev. Lett. **106**, 131302 (2011).

[33] R. Bernabei *et al.*, Eur. Phys. J. C **56**, 333 (2008).

[34] C. Savage, G. Gelmini, P. Gondolo, and K. Freese, J. Cosmol. Astropart. Phys. 04 (2009) 010.

[35] C. E. Aalseth *et al.*, Phys. Rev. Lett. **106**, 131301 (2011).

[36] E. Aprile *et al.*, Phys. Rev. Lett. **109**, 181301 (2012); M. Schumann (XENON100 Collaboration) (private communication).

[37] M. Felizardo *et al.*, Phys. Rev. Lett. **108**, 201302 (2012).

[38] S. Sivertsson and J. Edsjö, Phys. Rev. D **85**, 123514 (2012).

[39] Y. Bai, P. J. Fox, and R. Harnik, J. High Energy Phys. 12 (2010) 048.

[40] J. Goodman, M. Ibe, A. Rajaraman, W. Shepherd, T. M. P. Tait, and H.-B. Yu, Phys. Lett. B **695**, 185 (2011).

[41] P. J. Fox, R. Harnik, J. Kopp, and Y. Tsai, Phys. Rev. D **85**, 056011 (2012).

[42] H. Silverwood, P. Scott, M. Danninger, C. Savage, J. Edsjö, J. Adams, A. M. Brown, and K. Hultqvist, arXiv:1210.0844v2 [J. Cosmol. Astropart. Phys. (to be published)].

[43] ATLAS Collaboration, Report No. ATLAS-CONF-2012-033, 2012; CMS Collaboration, Report No. CMS-PAS-SUS-11-024, 2012; CMS Collaboration, arXiv:1207.1798.